Journal of Power Sources 187 (2009) 85–89

Contents lists available at ScienceDirect

Journal of Power Sources

journal homepage: www.elsevier.com/locate/jpowsour

Short communication

Evaluation of $Sr_{0.88}Y_{0.08}TiO_3$–CeO_2 as composite anode for solid oxide fuel cells running on CH_4 fuel

Xiufu Sun*, Shaorong Wang, Zhenrong Wang, Jiqin Qian, Tinglian Wen, Fuqiang Huang

Shanghai Institute of Ceramics, Chinese Academy of Sciences, 1295 Dingxi Road, Shanghai 200050, PR China

ARTICLE INFO

Article history:
Received 15 October 2008
Accepted 20 October 2008
Available online 28 October 2008

Keywords:
Solid oxide fuel cells
Anode
$SrTiO_3$
Methane fuel

ABSTRACT

$Sr_{0.88}Y_{0.08}TiO_3$ (YST) was synthesized and the performance of a YST–CeO_2 composite as an alternative anode for the direct utilization of CH_4 in solid oxide fuel cells (SOFCs) was investigated. X-ray diffraction showed that YST had good chemical compatibility with CeO_2 and YSZ (8 mol% Y-doped ZrO_2). The shrinkage of the YST–CeO_2 composite on sintering was less than that of pure YSZ and CeO_2, and its thermal-expansion behavior was similar to that of YSZ. With YSZ as electrolyte, ScSZ (10 mol% Sc-doped ZrO_2)–LSM ($La_{0.8}Sr_{0.2}MnO_3$) as cathode, and YST–CeO_2 composite as anode, single cells were prepared and tested in both H_2 and CH_4. The maximum power density obtained at 900 °C was 161.7 mW cm^{-2} in H_2 atmosphere and 141.3 mW cm^{-2} in CH_4. The results demonstrated the potential of using YST–CeO_2 composite as the anode for SOFCs.

1. Introduction

The development of ceramic anodes for the direct use of hydrocarbon fuels is becoming an important task in solid oxide fuel cell (SOFC) development [1]. It is attractive to produce electricity directly from hydrocarbon fuels, as this would provide a cheaper and more convenient way of using SOFCs. The state-of-the-art SOFC anode is Ni based cermet, which has excellent performance in H_2 and syngas, but is not suitable for using hydrocarbons directly due to the problem of carbon deposition. Also Ni-based anodes are likely to suffer structural damage when cycled repeatedly in oxidizing and reducing atmospheres [2–5]. Therefore, new anode materials are required to replace Ni-based anodes.

Many efforts have been made to develop these new anode materials, such as CeO_2 [6,7], doped $LaCrO_3$ [8,9], and $Sr_2Mg_{1-x}Mn_xMoCo_{6-\delta}$ with double perovskite structure [10]. Among these materials, CeO_2-based anodes have shown considerable promise for the direct oxidation of CH_4. However, they have not replaced Ni/YSZ (8 mol% Y-doped ZrO_2) anodes because of their relatively low electronic conductivity and the lattice expansion associated with the loss of oxygen under anodic conditions [11].

It has been reported that doped $SrTiO_3$ possesses good electrical and thermal properties as the anode in SOFCs [12,13]. Moreover, this material has been found to be dimensionally stable during oxidation–reduction cycling. However, doped $SrTiO_3$ shows poor electro-catalytic activity towards hydrogen and methane.

The addition of CeO_2 to doped $SrTiO_3$ can combine the advantages of these two materials [1,14]. In our previous work, we reported that a fuel cell with an anode consisting of $Sr_{0.6}La_{0.4}TiO_3$ and 50 wt% ratio of CeO_2 had the best performance [15]. In this paper, a composite anode made up of 8 mol% Y-doped $SrTiO_3$ mixed with 50 wt% CeO_2 has been prepared. Its chemical compatibility, sintering behavior and thermal expansion have been investigated. With YSZ as electrolyte, ScSZ (10 mol% Sc-doped ZrO_2)–LSM ($La_{0.8}Sr_{0.2}MnO_3$) as cathode, and YST–CeO_2 composite as anode, single cells have been prepared and their performance and long-term stability have been tested in both H_2 and CH_4.

2. Experimental

2.1. Sample preparation

$Sr_{0.88}Y_{0.08}TiO_3$ (YST) was prepared by the solid-state reaction method. The starting materials were as follows: $SrCO_3$ (99.8%, Sinopharm Chemical Reagent Co. Ltd.), TiO_2 (99.8%, Hubei Xiantao Zhongxing Electronic Material Co. Ltd.), and Y_2O_3 (99.99%, Rare-chem Hi-Tech Co. Ltd.). First, the raw materials were mixed in an appropriate molar ratio by ball milling for 4 h with ethanol. After drying, the mixture was calcined at 1150 °C for 3 h in air. The calcined sample was then ball milled with ethanol again for 3 h with CeO_2 (99.99%, Rare-chem Hi-Tech Co. Ltd.) in a 1:1 weight ratio to prepare the material for the composite anode.

The calcination was investigated based on TG–DSC analysis by a NETZCH SATA 449C apparatus with a heating rate of 5 °C min^{-1}.

* Corresponding author. Tel.: +86 21 52411520; fax: +86 21 52413903.
E-mail address: sunxf@mail.sic.ac.cn (X. Sun).

0378-7753/$ – see front matter.
doi:10.1016/j.jpowsour.2008.10.067

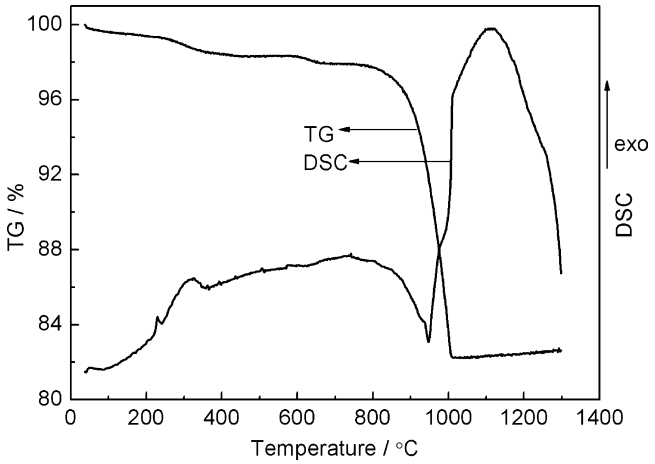

Fig. 1. TG–DSC analysis of the synthesis of YST.

Phase identification of synthesized samples was performed by X-ray diffraction analysis (Rigaku D/max 2550 V) with Cu Kα radiation and an Ni filter. To study the chemical compatibility of YST with CeO_2 and YST with YSZ, YST and the corresponding powders were mixed in a 1:1 weight ratio then sintered at 1350 °C for 3 h in air. The sintering process and thermal-expansion behavior of YST–CeO_2 were studied by dilatometer analyses with a NETZCH DIL 420C at a heating rate of 5 °C min^{-1} up to 1350 °C.

2.2. Fuel-cell preparation

To make the fuel cells, YST–CeO_2 slurry was prepared by mixing the YST–CeO_2 composite with terpilenol and ethyl cellulose. The slurry was screen printed onto the 0.3 mm thick dense YSZ electrolyte, followed by sintering at 1350 °C for 3 h. ScSZ and LSM mixtures with 30:70 weight ratio were used to make the cathode by screen printing and sintering at 1200 °C for 3 h. Au paste was used as the current collector. Each cell with a cathode area of 1.33 cm^2 was sealed onto an alumina tube via a glass ring. The fuel cell was then placed inside a furnace and heated to 900 °C. H_2 or CH_4 with 3% H_2O was fed to the anode side with a flow rate of 25 mL min^{-1} and O_2 was fed to the cathode side at the same flow rate. Before the fuel cell test, the anode was reduced in H_2 at 900 °C for 3 h. The current–voltage (*I–V*) curves and electrochemical impedance spectra (EIS) were obtained by an IM6e-X (ZAHNER, Germany) apparatus with 20 mV ac amplitude over the frequency range 8 mHz to 1 MHz. The performance of the fuel cell was tested in H_2 and CH_4. Between the two tests, the cell was purged with N_2 for at least 2 h with a flow rate of 25 mL min^{-1}. The anode microstructure was observed after the cell tests using a scanning electron microscope (SEM, JSM-6700F).

3. Results and discussion

3.1. TG–DSC and X-ray analyses

The TG–DSC curves of the YST sample are shown in Fig. 1. A sharp endothermic peak appears at 947.3 °C, corresponding to the decomposition of $SrCO_3$ to SrO and CO_2, accompanied by weight loss. This process continues up to 1020 °C. Then a broad exothermic peak appears at 1100 °C. The newly produced SrO has very high reactivity and reacts with TiO_2 to form $SrTiO_3$. Meanwhile, Y_2O_3 dissolves into it to form a solid solution. The reaction that takes place during this process in a wide range of temperature can be

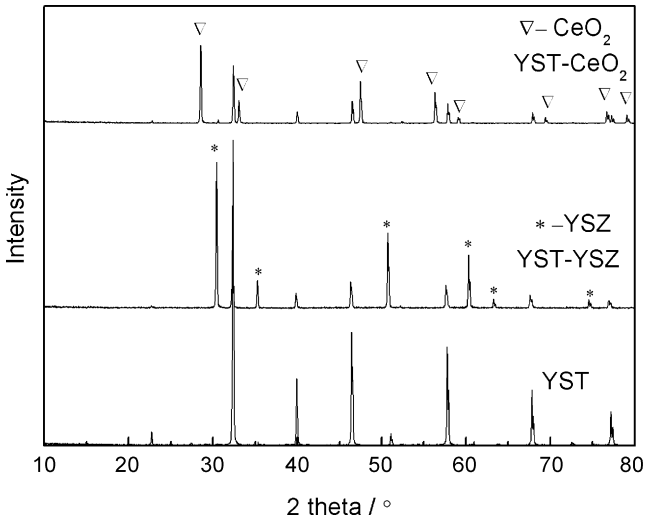

Fig. 2. X-ray diffraction patterns of YST, YST–CeO_2, and YST–YSZ.

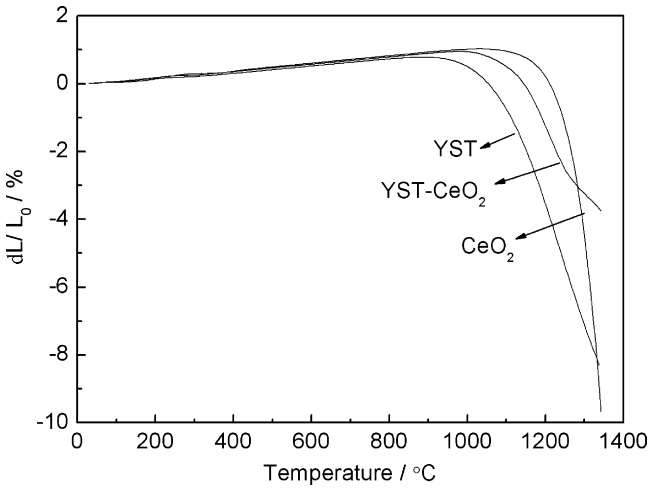

Fig. 3. Sintering characteristics of YST, CeO_2, and YST–CeO_2.

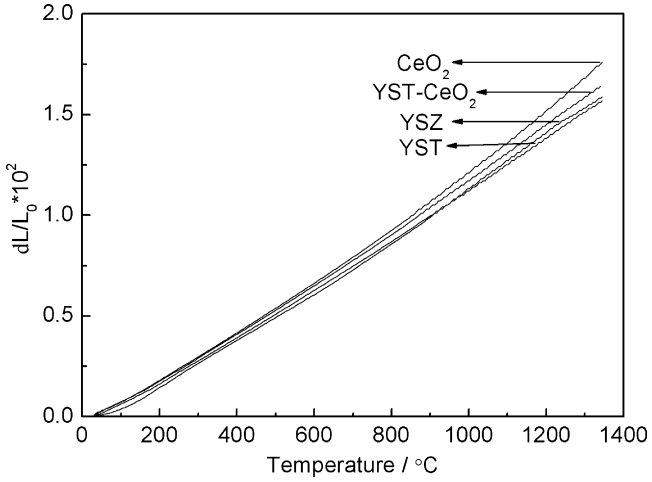

Fig. 4. Thermal-expansion behavior of YST, CeO_2, YST–CeO_2, and YSZ.

written as $(1-1.5x)\ SrO + TiO_2 + 0.5x\ Y_2O_3 \rightarrow Sr_{1-1.5x}\ V''_{0.5x}\ Y_xTiO_3$. Therefore, in order to get a single phase of YST, the powder was calcined at 1150 °C for 2 h.

Fig. 2 shows the X-ray diffraction patterns of YST, and YST–CeO_2, YST–YSZ mixtures (mixed with 1:1 ratio and then calcined at 1350 °C). It can be seen that the formation of $SrTiO_3$ and the dissolution of Y_2O_3 into $SrTiO_3$ are completed after calcination at 1150 °C for 2 h and the powder has a perovskite structure similar to the standard pattern of $SrTiO_3$ (JCPDS No.35-0734). The X-ray diffraction patterns show that after calcining at 1350 °C, there is no significant reaction between YST and YSZ, or between YST and CeO_2.

3.2. Sintering characteristics and thermal-expansion behavior

Fig. 3 shows the sintering characteristics of YST, CeO_2, and YST–CeO_2 measured from room temperature to 1350 °C in air. The shrinkage ratios of YST, CeO_2, and YST–CeO_2 are 10.3%, 8.5%, and 3.8%, respectively. The addition of CeO_2 significantly suppresses the sintering of YST.

The thermal-expansion behavior in air of YST, CeO_2, YST–CeO_2, and YSZ is shown in Fig. 4. YST–CeO_2 expands almost linearly in the temperature range 100–900 °C. The average thermal-expansion coefficients calculated between 30 and 900 °C are 11.47, 11.63, 12.22, and 11.04 (in $10^{-6}\ K^{-1}$ units) for YST, YST–CeO_2, CeO_2, and YSZ, respectively. The thermal expansion of YST–CeO_2 is lower than that of CeO_2, but a little higher than that of YST and YSZ.

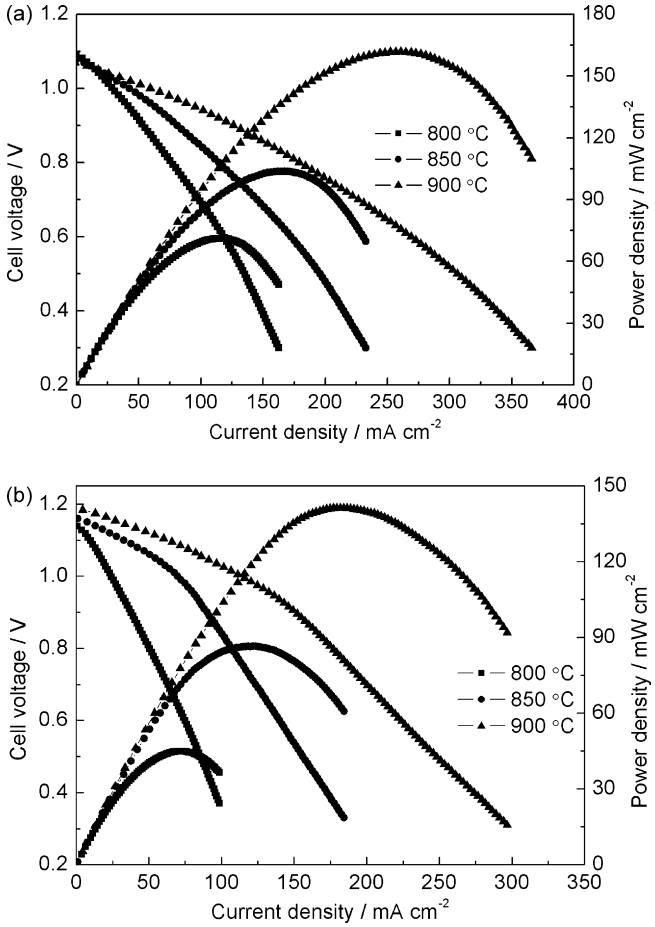

Fig. 5. *I–V* curves of the single fuel cell with YST–CeO_2 anode at different temperatures: (a) in H_2 + 3% H_2O fuel; (b) in CH_4 + 3% H_2O fuel.

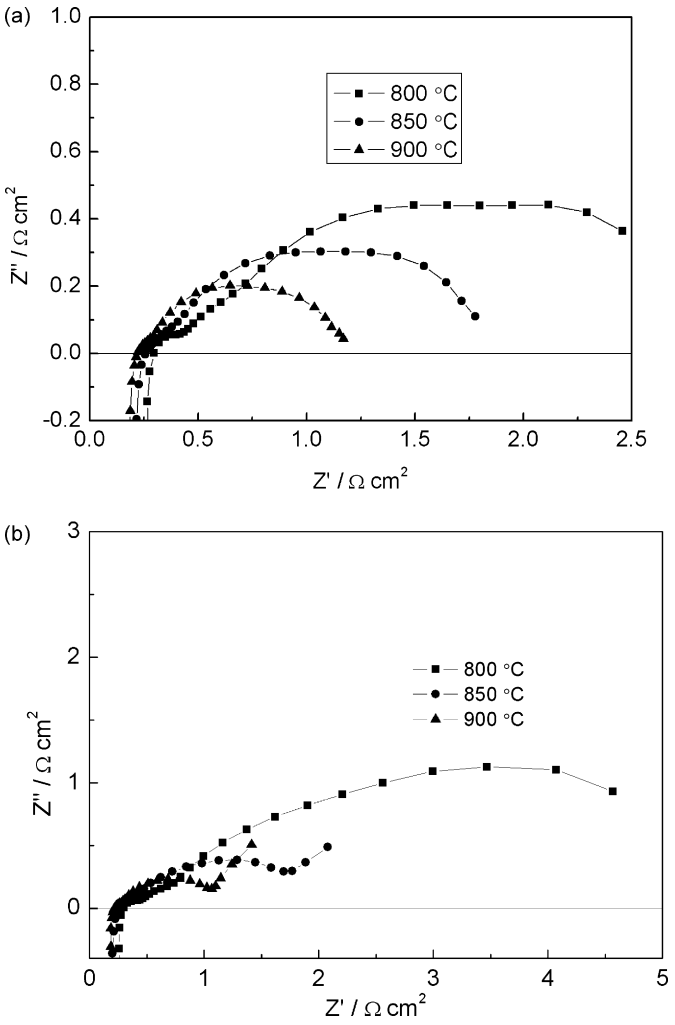

Fig. 6. Nyquist plots of the EIS under open-circuit conditions of the fuel cell at different temperatures: (a) in H_2 + 3% H_2O fuel; (b) in CH_4 + 3% H_2O fuel.

3.3. Fuel-cell performance in H_2 and CH_4

Single-cell tests were performed on electrolyte-supported cells with H_2 and CH_4 as fuel. The performance of the fuel cell running on H_2 and CH_4 at different temperatures is shown in Fig. 5(a) and (b). As the temperature increases from 800 to 900 °C, the open-circuit voltage decreases from 1.091 to 1.07 V in H_2, but increases from 1.138 to 1.184 V in CH_4. The maximum power densities of the fuel cell at 800, 850, and 900 °C are 71.1, 103.8, and 161.7 mW cm^{-2} in H_2, and 44.9, 86.5, and 141.3 mW cm^{-2} in CH_4, respectively.

In an attempt to examine the performance of the fuel cell at different temperatures, we measured the EIS of the cell running on H_2 and CH_4. Fig. 6(a) shows the impedance spectra of the fuel cell running on H_2. The ohmic resistances R_Ω, corresponding to the real-axis intercept at high frequency, are 0.297, 0.268, and 0.222 Ω cm^2, and the cell polarization resistances R_p, corresponding to the lower-frequency intercept, are 2.483, 1.462, and 0.852 Ω cm^2 at 800, 850, and 900 °C, respectively. The impedance spectra of the same cell running on CH_4 are shown in Fig. 6(b). At 800, 850, and 900 °C, the R_Ω calculated from the electrochemical impedance spectra are 0.298, 0.264, and 0.220 Ω cm^2, which are the same as in H_2, but the R_p values of the cell are 5.41, 1.66, and 0.905 Ω cm^2, which are larger than in H_2. With decreasing temperature, the R_p values of the cell increase faster than the ohmic resistance. The R_p in CH_4 fuel is larger than that in H_2, showing that CH_4 has more difficulty in completing

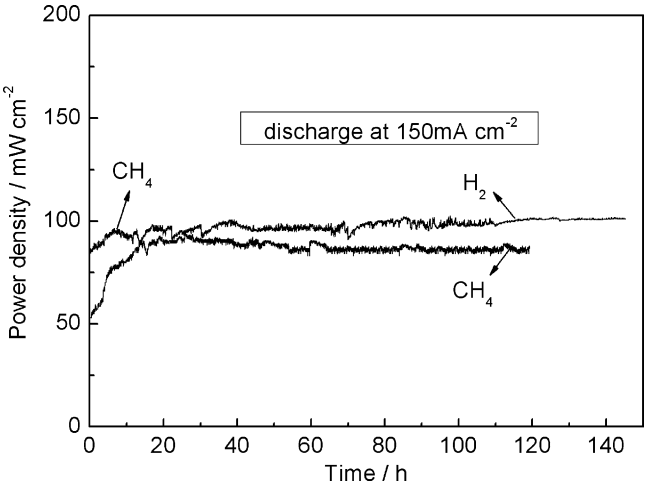

Fig. 7. Power density at 150 mA cm^{-2} as a function of time for the fuel cell running on H_2 and CH_4 at 900 °C.

the electrode reaction compared with H_2. At 900 °C, however, the polarization resistance does not differ so much between H_2 and CH_4, so a higher operation temperature is preferred for direct CH_4 feeding.

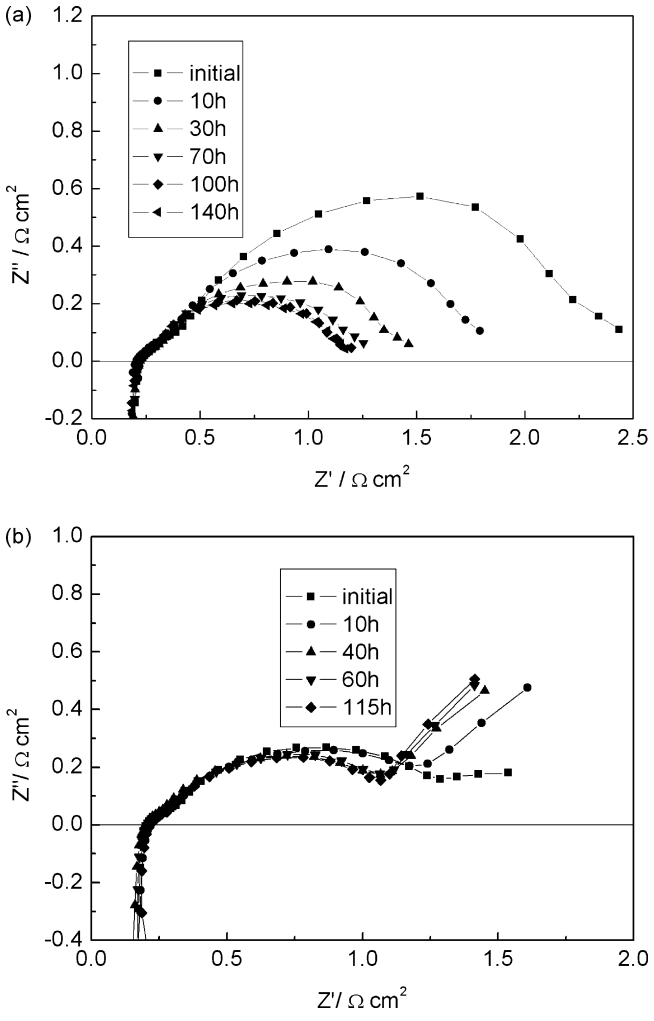

Fig. 8. Impedance spectra of the fuel cell as a function of operating time: (a) in H_2 + 3% H_2O fuel; (b) in CH_4 + 3% H_2O fuel.

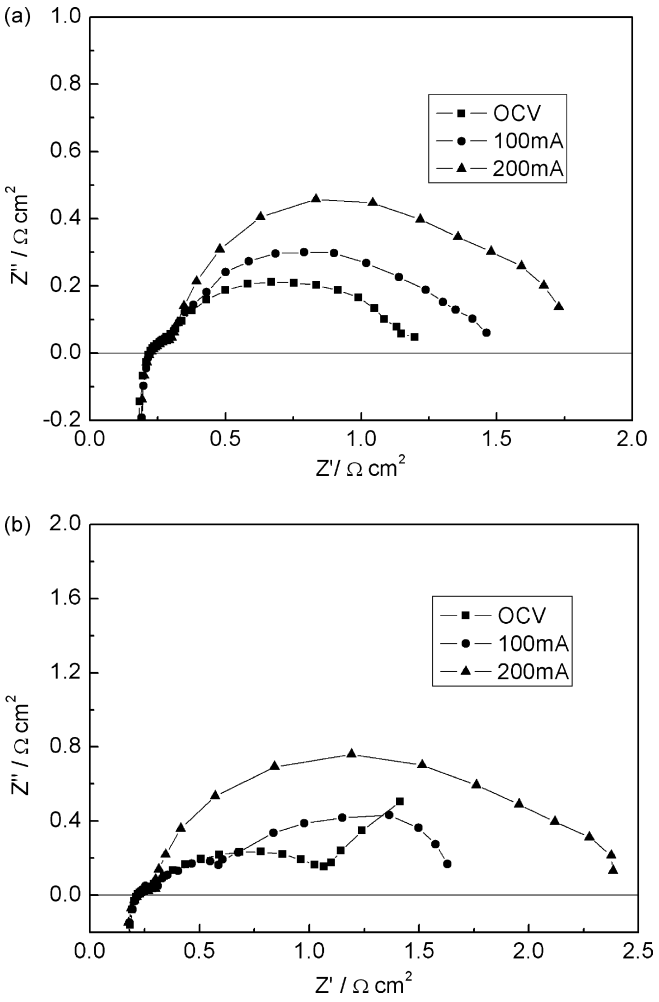

Fig. 9. Nyquist plots of the EIS at different discharge currents: (a) in H_2 + 3% H_2O fuel; (b) in CH_4 + 3% H_2O fuel.

The fuel-cell discharge characteristics at 150 mA cm^{-2} in H_2 and CH_4 at 900 °C are presented in Fig. 7. While running on H_2, the power density initially keeps on increasing. This process lasts for about 40 h, and may be due to the activation process of the LSM–SSZ cathode. Thereafter, the power density of the fuel cell stays constant at about 100 mW cm^{-2} with discharge at 150 mA cm^{-2}, and no degradation over a period of 145 h.

After about 145 h running on H_2, the fuel was switched to CH_4 after the cell had been purged with N_2 for about 2 h. The fuel cell discharged at 150 mA cm^{-2} for about 120 h in CH_4 and the power density remained constant at about 90 mW cm^{-2}.

During the operating period, the EIS of the fuel cell under open-circuit conditions were measured in order to get more information about the fuel-cell performance. The spectra of the fuel cell running on H_2 are shown in Fig. 8(a). The cell polarization resistance decreases with increasing discharge time up to 40 h, then remains constant until 145 h. When the fuel was switched to CH_4, as can be seen from Fig. 8(b), after about 10 h, the fuel polarization resistance stays constant for the rest of the discharge time. Since the YST–CeO_2 composite is a ceramic, it does not promote carbon deposition, so this anode material is very stable in a methane atmosphere.

In order to understand further the performance of the fuel cell, we measured the EIS at different discharge currents in H_2 and CH_4 fuel, respectively. As shown in Fig. 9(a) and (b), with increasing

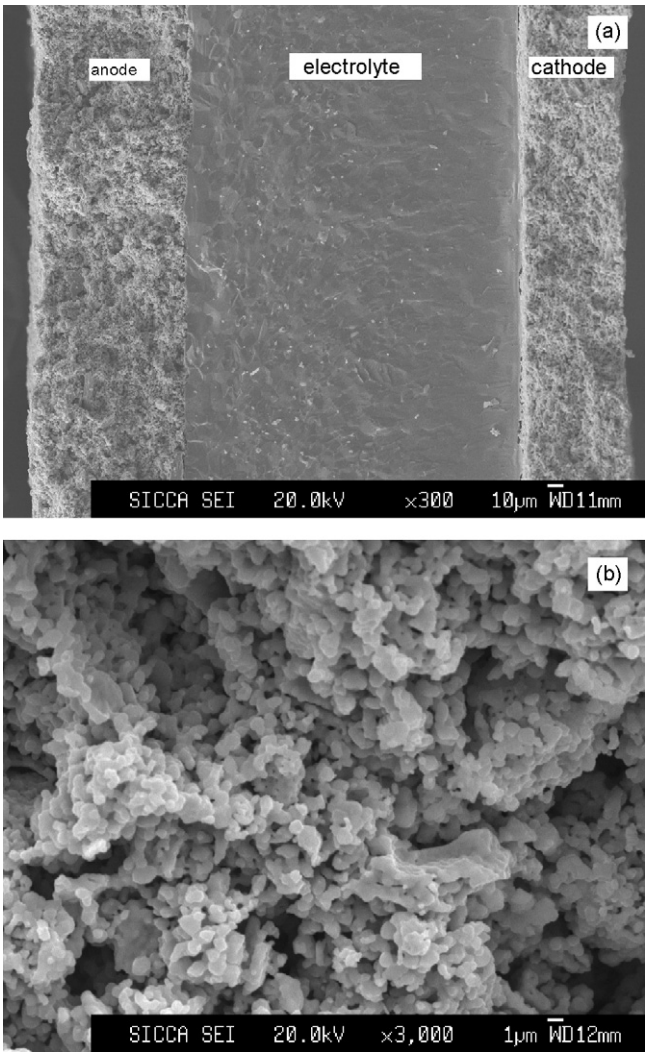

Fig. 10. Cross-sectional SEM images of the fuel cell: (a) YST–CeO_2/YSZ/LSM–SSZ single cell; (b) YST–CeO_2 anode.

discharge current, the ohmic resistance remains stable but the cell polarization resistance increases. This may result from some electrochemical process, such as mass transfer or the low electrical conductivity of the anode. In open-circuit conditions, there is a bigger arc in the low-frequency zone in Fig. 9(b) due to the lower mass-transfer speed of CH_4. But with increasing discharge current, this lower-frequency arc decreases. Comparing Fig. 9(b) with Fig. 9(a), it seems that the discharge current is good for reforming the CH_4. At a higher discharge current, more H_2 is produced. Therefore, the mass-transfer process is mainly dominated by H_2 rather than CH_4.

3.4. SEM observations

Fig. 10 shows cross-sectional SEM images of the YST–CeO_2/YSZ/LSM–SSZ interfaces (a) and the YST–CeO_2 anode (b). As shown in Fig. 10(a), the porous anode layer and the dense electrolyte layer are in good contact without obvious segregation. A tight junction can be seen at the interface between the electrolyte and the cathode layer. The thickness of the anode is about 100 μm. Fig. 10(b) shows that the small YST–CeO_2 particles have a homogenous pore distribution.

4. Conclusion

Y-doped $SrTiO_3$ perovskite oxide was synthesized and its compatibility with CeO_2 and YSZ was examined. With YSZ as electrolyte, ScSZ (10 mol% Sc-doped ZrO_2)–LSM ($La_{0.8}Sr_{0.2}MnO_3$) as cathode, and YST–CeO_2 composite as anode, single cells were prepared and tested in both H_2 and CH_4. As the temperature increased from 800 to 900 °C, the maximum power density improved from 71.1 to 161.7 mW cm^{-2} in H_2 and from 44.9 to 141.3 mW cm^{-2} in CH_4. The electrochemical impedance spectra demonstrated that with increasing temperature, the cell polarization decreased remarkably. The YST–CeO_2 anode showed very good stability during 145 h of operation in H_2 and 115 h of operation in CH_4 fuels. These results demonstrated that YST–$x$$CeO_2$ composites can be considered as potential anode materials for SOFCs directly utilizing hydrocarbon fuels.

Acknowledgement

The authors gratefully acknowledge financial support from the Chinese Government High Tech Development Project (2007AA05Z151).

References

[1] S. Koutcheiko, Y. Yoo, A. Petric, I. Davidson, Ceram. Int. 32 (2006) 67–72.
[2] O.A. Marina, L.R. Pederson, 5th European Solid Oxide Fuel Cell Forum, Lucerne, 1–5 July, 2002.
[3] Q.X. Fu, F. Tietz, D. Stover, J. Electrochem. Soc. 153 (2006) D74–D83.
[4] R.J. Gorte, H. Kim, J.M. Vohs, J. Power Sources 106 (2002) 10–15.
[5] J.B. Goodenough, Y.H. Huang, J. Power Sources 173 (2007) 1–10.
[6] S. An, C. Lu, W.L. Worrell, R.J. Gorte, J.M. Vohs, Solid State Ionics 175 (2004) 135–138.
[7] Z.L. Zhan, S.A. Barnett, Science 308 (2005) 844–847.
[8] S.P. Jiang, X.J. Chen, S.H. Chan, J.T. Kwok, K.A. Khor, Solid State Ionics 177 (2006) 149–157.
[9] V.V. Kharton, E.V. Tsipis, I.P. Marozau, A.P. Viskup, J.R. Frade, J.T.S. Irvine, Solid State Ionics 178 (2007) 101–113.
[10] Y.H. Huang, R.I. Dass, Z.L. Xing, J.B. Goodenough, Science 312 (2006) 254–257.
[11] M. Mogensen, T. Lindegaard, U.R. Hansen, G. Mogensen, J. Electrochem. Soc. 141 (1994) 2122–2128.
[12] O.A. Marina, N.L. Canfield, J.W. Stevenson, Solid State Ionics 149 (2002) 21–28.
[13] S.Q. Hui, A. Petric, Mater. Res. Bull. 37 (2002) 1231–1251.
[14] O.A. Marina, L.R. Pederson, M.C. Williams, G.W. Coffey, K.D. Meinhardt, C.D. Nguyen, E.C. Thomsen, J. Electrochem. Soc. 54 (2007) B452–B459.
[15] X.F. Sun, S.R. Wang, Z.R. Wang, X.F. Ye, T.L. Wen, F.Q. Huang, J. Power Sources 183 (2008) 114–117.